Progress report

Experimental studies of reactions induced by ^{3}He on targets of ^{10}B, ^{11}B, and ^{7}Li

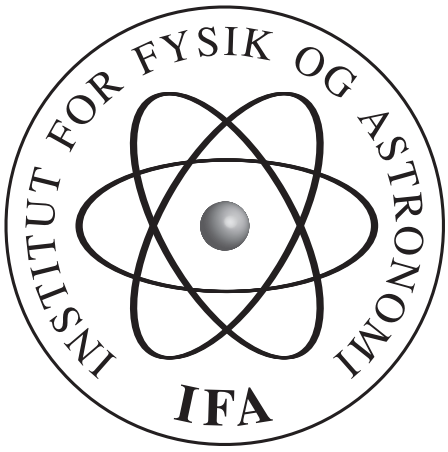

Oliver S. Kirsebom

Institute of Physics and Astronomy, University of Aarhus

May 19, 2008

Contents

About me and my studies

The process of learning is a funny thing. You may be able to follow each step in a long and complicated explanation, yet at the end of it all you may be left with a feeling that you have not *understood* the argument as a whole. The grand picture is still missing. I often have this experience when introduced to unfamiliar fields of physics. It just takes time for new information to settle. By working on the problems yourself, solving them using the same methods over and over again, what initially seemed very complicated becomes clear and you eventually begin to feel that you understand many things. Practice and experience are essential to the process of learning new things.

I started as a PhD student in the subatomic group at the University of Aarhus in August 2006. During the past two years I have had the chance to participate in a number of experiments at various locations. At ISOLDE we have done transfer reactions to study light neutron-rich beryllium isotopes, we have looked at the beta-delayed particle break-up of ^{17}Ne and ^{11}Li, and done lifetime measurements of the alpha-unstable isotopes ^{221}Fr, ^{224}Ra, and ^{226}Ra in various enviroments. In Grenoble I took part in an experiment, which aimed at measuring the lifetime of a certain isomeric state in ^{12}Be produced in the fission reactor at ILL. Recently we have studied the beta-decay of ^{8}B both at KVI in Groningen, Netherlands, and at the IGISOL facility in Jyväskylä, Finland, using two different detection methods. Finally we have performed a series of experiments at the CMAM facility in Madrid with a stable ^{3}He beam on ^{7}Li, ^{10}B, and ^{11}B targets. In addition to the experimental work I have attended a number of conferences and schools and I was even given the opportunity to spend about one month at the Tokyo Institute of Technology on a foreign graduate student program.

Unfortunately I will not be telling you about these trips that make life as a PhD student in experimental nuclear physics quite tolerable, nor will I have time to discuss all the interesting physics that we have studied in many of our experiments. Rather I will spend most of this progress report to present my analysis of our Madrid experiments where, as I mentioned, we have studied the nuclear reactions that occur when a beam of ^{3}He ions hit targets made of ^{7}Li, ^{10}B, and ^{11}B. During the time I have been part of the subatomic group in Aarhus I have learned a great deal about the details of these reactions. In my analysis I have repeatedly been using a large number of tools and methods commonly used in the sub-branch of nuclear physics dealing with low-energy reactions of light nuclei. Eventually I have come to understand much of the physics that seemed complicated at the beginning and looking back it may sometimes be difficult to understand how it could take so long to get to the point where I find myself now. It is my hope that I will be able to put some of this understanding down in words and convey it in a clear and interesting way to the person who happens to be reading this report.

I shall start by explaining what it is we hope to learn about the subatomic world from our reaction studies in Madrid (chapter 1). Then I will go through the experimental setup (chapter 2), discuss the simulations (chapter 3), and present the results of my analysis (chapter 4). Finally I intend to say a few words about my plans for the next two years.

Chapter 1

An introduction to the physics

Various models are being used to interprete the properties of the states observed in nuclei. One model may be applicable to nuclei in a certain region of the nuclear chart, while a different model must be used to explain the behavior observed in another part of the nuclear chart. These models often focus on different aspects of the nucleus and in some cases supplement each other to achieve the full picture.

The liquid drop model, for instance, explains the various terms appearing in the Weizsäcker's mass formula, which proves successful in predicting the binding energy of nuclei depending on the number of protons Z and neutrons N. The shell model focuses on single particle degrees of freedom. The nucleons are assumed to move around in an average central potential without interacting, hence they occupy single particle orbits of fixed energy, orbital angular momentum and spin. In the nuclear ground state the single particle orbits are filled up according to the Pauli exclusion principle starting from the bottom. It is not easy to see why this model should work as well as it actually does. With the addition of a strong spin-orbit coupling to the radial potential the shell model is able to predict important nuclear properties such as spin-parity of odd A and even-even nuclei as well as the observed magic numbers corresponding to closed shells. Residual interactions may be included in the model. The ground state then no longer corresponds to a single spectroscopic configuration but a linear combination of many, an effect known as configuration mixing. Due to the short range of the nuclear force it would seem reasonable to assume the shell model central potential to have the same radial dependence as the nuclear density. However, the nuclear density itself is determined by the form of the potential. Standard methods commonly known as the Hartree-Fock method exist to tackle this problem.

In the closed shell configuration the nuclei tend to be spherical, but deformations grow as more nucleons are added and collective degrees of freedom appear. The nucleons may now be thought of as moving inside an ellipsoidal box, which itself may either rotate or vibrate. The nucleons, now moving in a non-central potential, still occupy single particle orbits, but the ordering of the levels can change. The collective motion of the nucleus leads to additional nuclear states, for instance in even-even nuclei rotational bands of spin-parity 0^+, 2^+, 4^+, etc. appear in the excitation spectrum (a rotation of 180 degrees is sufficient to restore the original configuration, this explains why a 0^+ state only generates even spin-states). The giant dipole resonance is another example of a collective degree of freedom. In this case all protons together oscillate relative to the neutrons.

Obviously one would like to derive the observed nuclear properties from a basic nucleon-nucleon interaction. This approach introduces plenty degrees of freedom many of which are irrelevant to the problem and hence becomes computationally very demanding.

Presently such computations have been carried out up to mass number 12. While excited states have been calculated for stable nuclei up to $A = 11$ only the ground state has been computed in the case of ^{12}C. Unfortunately the prospects for further advancements are limited since the computational power required beyond mass 12 increases dramatically. These methods also face problems when dealing with unbound states. The starting point of such ab-initio calculations is a so-called realistic nucleon-nucleon force, which depends on the positions, velocities, spins and isospins of the interacting nucleons. The expression normally includes all terms compatible with lorentz invariace, symmetries of space (translation and rotation), and symmetries of the nuclear force (parity and isospin), which adds up to a total of eight terms, each multiplied with a function of r determined by scattering experiments and measured properties of the deuteron. It turns out that a phenomenological three-body force must be added to make things work, even in the case of ^{3}He and ^{3}H. Some people take an even more fundamental approach and try to derive an expression for the nucleon-nucleon interaction from QCD.

1.1 The α-cluster model

Having already mentioned a number of nuclear models there is still one which also has to be mentioned here namely the alpha-cluster model, since it provides important motivation for the experimental studies to be presented in this report. In the alpha-cluster model the basic building blocks are not single nucleons but helium cores with spin-parity 0^+ and no internal degrees of freedom. From a suitable choice of alpha-alpha potential it is then possible to calculate properties of the $N\alpha$ nuclei ^{8}Be, ^{12}C, ^{16}O, ^{20}Ne, ^{14}Mg and so on. With three or more alphas present in the core three-body or non-local forces must be included to account for the dependence of the alpha-alpha interaction on changes in the alpha-structure induced by the interaction with the third "observer" alpha. The alpha-cluster model possesses an appealing simplicity. While reducing the number of degrees of freedom compared to the ab-initio method it retains the essential idea of ab-initio calculations namely to understand the nucleus in terms of its building blocks and their mutual interaction. Due to the unusually large binding energy of the helium core it seems reasonable to hope that the alpha-cluster model may be successful, however only by comparing its prediction to experiments will we know.

The idea of alpha-clusters was already coined in the 1930's by Wheeler and others [Wh37]. Years later Morinaga [Mo56] applied the alpha-cluster model to the light $N\alpha$ nuclei in an attempt to explain their low-energy level structure, which is not easy to understand from simple shell model theories. At the time Morinaga wrote his paper a low-lying 0^+ state was known to exist in both ^{12}C, ^{16}O, ^{20}Ne, and ^{14}Mg. While the ground state would correspond to a compact cluster of N alpha particles, Morinaga proposed that this low-lying 0^+ state could be described as a rotationless linear chain of N alpha particles. The rotation of such a structure would lead to a band of excited states with spin-parity 2^+, 4^+, etc. on top of the rotationless 0^+ state. It would also be possible for such a structure to vibrate thereby leading to additional energy levels. By some simple calculations based on a semi-classical and crude model in which the linear structure of N alpha particles was treated as a rigid rotator with a fixed moment of inertia, Morinaga was able to give rough estimates on the energy of the 0^+ state and make predictions on the relative spacing of its rotational excitations. When compared to the data his model gave reasonable predictions for ^{16}O, ^{20}Ne, and ^{14}Mg, but experimental evidence was definitely not conclusive. As for ^{8}Be and ^{12}C even less was known and the data available certainly did not suffice neither to rule out nor verify the alpha-cluster model. The cluster-model has also been applied to nuclei such as ^{9}Be and ^{13}C which

are described as configurations of two and three alphas, respectively, plus an additional neutron [Ya04].

The low-lying 0^+ state in ^{12}C sits at 7.654 MeV and is well-known to astrophysicist because of its crucial role in helium-burning in stars. It was named after Fred Hoyle who in 1953 predicted its existence and properties to account for the observed abundances of ^{12}C and ^{16}O in the Universe [Ho53]. Assuming that Morinaga is right in his claim that the Hoyle state may be described as a linear chain of three alpha particles one would expect the existence of rotational 2^+ state at somewhat higher excitation energy. From his simple model Morigana estimated this hypothetical state to be situated about 9.7 MeV above the ground state. In 1958 a broad state at 10.1(2) MeV was indeed observed to be populated in the beta-decay of ^{12}B [Co58], which meant it had to be 0^+, 1^+, or 2^+. In 1966 the existence of this level was confirmed in another beta-decay experiment [Sc66], this time its energy was measured to be 10.3(3) MeV. Furthermore it was observed to decay through the ground state of ^{8}Be, which left 0^+ and 2^+ as the only possible spin-parity assignments. When Morinaga learned that a broad state at 10.3 MeV had been seen experimentally he suggested that this could be his 2^+ state [Mo66]. However, our own beta-decay studies [Fy05] support a 0^+ assignment in agreement with recent ^{12}C$(\alpha,\alpha')^{12}$C experiments [Be03, It04]. Additional states tentatively assigned as 2^+ have been observed experimentally (albeit only weakly populated) in the energy region predicted by Morinaga, see e. g. [Be03, It04, Fr07]. However these states were not seen in our experiment nor in any of the earlier beta-decay studies. We do find evidence for a 2^+ resonance near 14 MeV, but see no sign of the 2^+ state at 9.1 MeV that is currently included (on theoretical grounds) in the nuclear astrophysics compilation of reaction rates (NACRE) with significant astrophysical implications as discussed in [Fy05]. Faced with these conflicting observations we wanted to verify our own results by a different approach, and so we decided to perform a study the ^{10}B$(^3\mathrm{He}, p\alpha\alpha\alpha)$ reaction.

The low-energy level structure of ^{12}C is summarized in table 1.1. The first excited state sits at 4.44 MeV and has spin parity 2^+, it is also the only bound state in ^{12}C not counting the ground state obviously. The second excited state is the famous Hoyle state. It is situated only some few hundred of keV above the triple alpha threshold, hence its importance for the triple alpha reaction taking place in the interior of stars. As we go up in excitation energy many more states appear. In our beta-decay studies of ^{12}C selection rules only allowed the population of states with spin-parity 0^+, 1^+, and 2^+. In contrast the ^{3}He+^{10}B $\rightarrow p+^{12}$C reaction allows us to populate any state regardless of spin-parity, thus several states which were not accessible in the beta-decay experiment can now be studied. Furthermore, it has been argued that the absence of any 2^+ contribution in the ^{12}C spectrum obtained from beta-decay experiments could be accounted for by a weak feeding to the 2^+ state in beta-decay, which in turn would be explained by its pronounced alpha-cluster structure [Ka07]. However, if no 2^+ contribution is found in the reaction studies either, the validity of this explanation would be cast in doubt.

The 4.44 MeV state decays to the ground state by an E2 transition. The states above the triple alpha threshold normally decay by break-up into three alpha particles and have very small gamma branches to lower lying states at the percent level or below. This is not to say that the gamma branches are unimportant. In the case of the Hoyle state the existence of a 10^{-4} gamma branch is of essential importance. If there were no gamma branch no carbon would be produced in the triple alpha reaction since whenever formed the Hoyle state would immediately break-up into the three alphas again. The existence of a small gamma branch ensures that on a few occasions the Hoyle state decays to the ground state thereby forming stable carbon. Exceptions to the rule of small gamma widths exist. The 1^+ state at 15.11 MeV decays primarily by gamma emission and has an

E_x [MeV $\pm$ keV]	J^π	Γ [keV]	decay
g.s.	0^+	-	stable
4.43891 ± 0.31	2^+	$(10.8 \pm 0.6) \times 10^{-6}$	γ
7.6542 ± 0.15	0^+	$(8.5 \pm 1.0) \times 10^{-3}$	γ, π, α
9.641 ± 5	3^-	34 ± 5	γ, α
10.3 ± 300	(0^+)	3000 ± 700	α
10.844 ± 16	1^-	315 ± 25	α
(11.16 ± 50)	(2^+)	430 ± 80	
11.828 ± 16	2^-	260 ± 25	γ, α
12.710 ± 6	1^+	$(18.1 \pm 2.8) \times 10^{-3}$	γ, α
13.352 ± 17	(2^-)	375 ± 40	γ, α
14.083 ± 15	4^+	258 ± 15	α
15.110 ± 3	1^+	$(43.6 \pm 1.3) \times 10^{-3}$	γ, α
15.44 ± 40	(2^+)	1500 ± 200	
16.1058 ± 0.7	2^+	5.3 ± 0.2	γ, p, α
16.57	2^-	300	γ, p, α

Table 1.1: ^{12}C states [TUNL]. Brackets indicate tentative assignments.

alpha branch of no more than a few percent, which is actually isospin forbidden because the 15.11 MeV state has been assigned isospin $T = 1$. The existence of an isospin-violating alpha width is explained by mixing with the 12.71 MeV state, which also has spin-parity 1^+, but isospin $T = 0$. The alpha width of the 15.11 MeV state hence gives a measure of the degree of mixing between the two 1^+ states [Ba74]. From our beta-decay studies we obtained a value for the alpha width, which was somewhat lower than the value normally quoted in the litterature [TUNL]. Hopefully we will be able to confirm or dismiss this result with our new reaction studies. Decay by proton rather than alpha emission becomes energetically possible once the excitation energy exceeds 15.9 MeV.

In two-body decays the fragments emerge back-to-back with energies locked by energy and momentum conservation. In contrast the kinematics of three-body decays is not fully determined by the conservations laws and the energy and angular distributions of the fragments depend on the decay mechanism. A specific example will help elucidate my point. A number of models have been used to describe the decay of the 12.71 MeV state in ^{12}C into three alpha particles. One model assumes the decay to proceed directly to the final state without any alpha-alpha interaction (democratic decay). The presence of three identical bosons requires the final state wave function to be symmetric with respect to the exchange of any two alpha particles. Furthermore angular momentum must be conserved. A second model, known as the sequential model, describes the decay as a sequence of two two-body decays, where the 12.71 MeV state decays to the broad 2^+ resonance in ^{8}Be by alpha-emission, followed by the break-up of ^{8}Be(2^+) itself into two alphas. Any dynamic interaction between particles emitted at different stages of the decay is neglected, and the only correlations are due to the conservation of energy and angular momentum. In other words it is assumed that the motion of the first emitted alpha is not perturbed by the two alphas emitted in the subsequent break-up of ^{8}Be. Notice that decay to the 0^+ ground state in ^{8}Be is parity-forbidden. The argument goes as follows. Since the alpha particle and the ^{8}Be ground state both are spin-0 while the initial ^{12}C state is spin-1 the decay has to proceed through a p-wave in order to conserve angular momentum. Both decay fragments have positive parity so the final state parity would then be $(+1) \times (+1) \times (-1)^l$ and hence negative when as argued $l = 1$. However the initial ^{12}C state happens to have positive parity so the decay is parity-breaking and

hence not possible by strong interactions. It turns out that the sequential model gives the best fit to the energy correlations observed between alphas emitted in the decay of the 12.71 MeV state, but systematic deviations suggest that alpha-alpha interactions in the final state cannot be neglected and a proper three-body description is needed [Fy03]. With the new reaction data we will be able to perform similar decay studies for any of the ^{12}C states populated in the $^3\mathrm{He} + {}^{10}\mathrm{B} \rightarrow p + {}^{12}\mathrm{C}$ reaction, which should allow us also to establish their spin-parity, which in some cases is not well-determined.

When the resonances that mediate the reaction are narrow and hence long-lived the interaction between final state particles may safely be ignored and the sequential model applies. However, in the case that we have just discussed the intermediate resonance is wide and hence short-lived, and the applicability of the sequential model comes as somewhat of a surprise. Assuming that the $^8\mathrm{Be}(2^+)$ resonance is produced at its nominal energy, 3.0 MeV above the ground state, the energy available to the two decay fragments in the break-up of the 12.71 MeV state is about 2.3 MeV, which corresponds to a relative velocity of 4% of the speed of light. This relative velocity is only obtained once the fragments have reached a separation where the electrostatic repulsion between the two is small. The width of the broad 2^+ state is $\Gamma = 1.5$ MeV corresponding to a life time of $\tau = \hbar/\Gamma = 4 \times 10^{-22}$ seconds. Together with the relative speed in the asymptotic limit this gives an upper estimate of $d = 0.04c \times \tau = 5$ fm on the average separation of the decay fragments at the instant when the ^{8}Be nucleus breaks up into two alphas. At this separation the nuclear forces are likely to be absent, but the coulomb repulsion is certainly not negligible, in fact the electrostatic energy between two alphas separated by only 5 fm equals $4\alpha\hbar c/d = 4 \times 200$ MeV fm$/(137 \times 5$ fm$) = 1$ MeV. In the light of this result it is surprising that the sequential model gives a good fit to the observations. Notice that at the time of the break-up the electrostatic energy in the $\alpha + {}^8\mathrm{Be}$ system is about 2 MeV, thus roughly equal to the kinetic energy of the fragments at infinity. If the break-up had occured only moments earlier it would, so to speak, have happened while the alpha particle was still in the process of tunneling under the Coulomb barrier. These considerations make it abundantly clear that the semi-classical approach offered by the sequential model breaks down when the intermediate resonances become too wide.

1.2 Studying ^{12}C with the $^{10}\mathrm{B}(^3\mathrm{He}, p\alpha\alpha\alpha)$ reaction

The $^{10}\mathrm{B}(^3\mathrm{He}, p\alpha\alpha\alpha)$ reaction was the subject of a thorough and comprehensive experimental investigation by Waggoner and his collaborators back in 1966 [Wa66]. Despite the technological limitations of those times they were able to extract an impressive amount of information from their studies. It was recognized that at beam energies of 2.45 and 6.0 MeV the reaction proceeds through three different channels

$$^{10}\mathrm{B} + {}^3\mathrm{He} \rightarrow \begin{cases} p + {}^{12}\mathrm{C},\ {}^{12}\mathrm{C} \rightarrow 3\alpha \\ \alpha + {}^9\mathrm{B},\ {}^9\mathrm{B} \rightarrow p + 2\alpha \\ {}^5\mathrm{Li} + {}^8\mathrm{Be},\ {}^5\mathrm{Li} \rightarrow p + \alpha,\ {}^8\mathrm{Be} \rightarrow 2\alpha \end{cases}$$

The $p+{}^{12}$C channel is the one we are after because it holds information on the structure of ^{12}C. With the center of mass energy fixed by the choice of beam energy, target, and projectile, the measured energy of the outgoing proton together with its angle of emission relative to the beam axis uniquely determines the ^{12}C excitation energy. Thanks to the large Q-value of the $^3\mathrm{He} + {}^{10}\mathrm{B} \rightarrow p + {}^{12}\mathrm{C}$ reaction (19.69 MeV) we may populate states in ^{12}C more than 20 MeV above the ground state with a modest choice of beam energy.

From the observation of the proton emitted in the $^3\mathrm{He} + {}^{10}\mathrm{B} \rightarrow p + {}^{12}\mathrm{C}$ reaction we may identify resonances in ^{12}C, determine their energy and total width and maybe

even learn something about the dynamics of the reaction that lead to the formation of the resonance by looking at the angular distribution of the proton. However, the proton does not hold any spin-parity information, nor can it tell us about the faith of the ^{12}C nucleus. Did it decay by alpha emission? If so, how did the decay proceed? Information on the decay mechanism can only be obtained from the detection of the decay products themselves.

Our detector setup (to be introduced in the following chapter) did not permit the detection of gamma rays, so the gamma decays of the 4.44 MeV state and the occasional gamma decays from states above the triple-alpha threshold could not be directly measured. However, we do observe the recoiling ^{12}C nucleus in coincidence with the proton and on such occasions the energy and direction of the emitted photon should be, at least in principle, possible to deduce from energy and momentum conservation.

1.3 Other aspects

Before ending this chapter a few remarks on the two remaining reaction channels identified by Waggoner and his collaborators in 1966 are appropriate. It is clear that the $\alpha + ^9$ B channel holds information on the structure and decay mechanism of states in ^{9}B and that this information may be extracted from the observed final state particles in much the same way as explained for ^{12}C. One case of particular interest is the decay mechanism of the $5/2^-$ state situated 2.36 MeV above the (unbound) ground state of ^{9}B. From Waggoners experiment this state is known to have a small proton width to the ^{8}Be ground state, but mostly it decays to the $p + \alpha + \alpha$ continuum by other mechanisms which are not well understood. One could imagine the decay to proceed through the low-energy tail of the broad 2^+ state in ^{8}Be. Alternatively the $5/2^-$ state could decay by alpha emission to the broad and unbound ground state of ^{5}Li which subsequently breaks up into a proton and an alpha. In both cases the decay is mediated by broad resonances which makes it very difficult to distinguish between the two channels. Furthermore the sequential picture may, as was already discussed, not be very meaningful under such circumstances. Another case of interest is the search for the isobaric analog to the $1/2^+$ state at 1.68 MeV in ^{9}Be, which has not yet been observed in ^{9}B. See [Fo06] for reference.

Even though Waggoner claims to observe the $^5\mathrm{Li} + ^8\mathrm{Be}$ channels in his experiment, the evidence he presents is in my oppinion far from conclusive. The broad nature of the intermediate resonances involved makes this channel difficult to identify in any incomplete kinematic measurement. While the experimental evidence presented by Waggoner certainly does not rule out a possible contribution from these channels, it does not prove their existence either. With our superior setup much stronger conclusions can be made about the contribution of these channels to the $^{10}\mathrm{B}(^3\mathrm{He}, p\alpha\alpha\alpha)$ reaction.

The setup used to study the $^{10}\mathrm{B}(^3\mathrm{He}, p\alpha\alpha\alpha)$ reaction has also been used to investigate reactions induced by the ^{3}He beam on targets made of ^{7}Li and ^{11}B. In the case of ^{7}Li our main interest lies with the $p + ^9$Be channel that among other things will allow us to study the decay mechanism of the $5/2^-$ state in ^{9}Be. The decay has previously been desribed in terms of a direct model with some success [Pr05], but recent experimental results [Pa07] seem to favour a sequential model going through the broad 2^+ resonance in ^{8}Be. In the case of ^{11}B our main focus is the $d + ^{12}$C channel which obviously will provide additional information on levels in ^{12}C.

Chapter 2

Experimental apparatus

The experimental study of the nuclear reactions induced by ^{3}He on targets of ^{10}B, ^{11}B, and ^{7}Li was performed at the CMAM facility (`http://www.cmam.uam.es/`) outside Madrid, Spain, which hosts a 5 MV terminal voltage tandem accelerator capable of delievering a very stable and well collimated beam of ^{3}He ions at intensities and energies that match our needs. The machine has a very good energy resolution of only a few eV. Charged particles emerging from the reaction site were observed in double sided silicon strip detectors (DSSSDs) backed by silicon pads for particle identification.

The ^{3}He + ^{10}B reaction was the only one to be studied when the first test run took place in spring 2005. One year later the actual experiment was performed with an improved setup. This time a few hours were devoted to the ^{7}Li target. The data collected on this occasion was handed to me a few months later when I joined the nuclear physics group in Aarhus as a PhD student. It soon became clear from my analysis that a repetition of the experiment would be worthwile the effort since the quality of the data and the amount of statistics could be significantly enhanced by some fairly small adjustments to the setup.

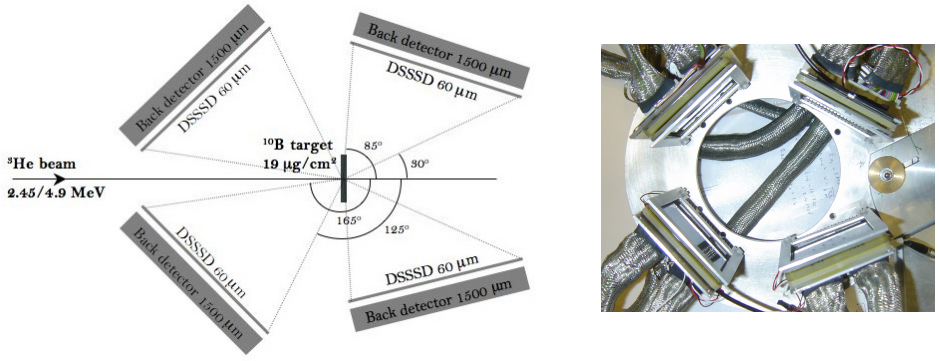

Figure 2.1: Detector setup in 2006.

In March this year the experiment was eventually repeated with an improved setup designed to maximize our acceptance to 4-coincidence events. The new design was based on loads of simulations as well as our experience from the two previous runs. The main difference compared to the 2006 setup shown in figure 2.1 was to move the small angle detectors closer to the beam line, because it was realised that this adjustment would greatly enhance the number of 4-coincindece events in the data. Generally speaking the trajectory of the protons is only lightly perturbed by the motion of the c. m. frame relative to the laboratory, because the protons are light, run off with a major part of the energy released in the reaction, and consequently have large c. m. velocities. In contrast the

alphas being heavy have small c. m. velocities and their motion in the laboratory frame is greatly perturbed if not completely dominated by the c. m. motion. As a consequence the alphas tend to be focused in the beam direction, which explains why our ability to observe 4-particle coincidences is enhanced by moving the detectors. The detectors were also placed closer to the target to increase the overall amount of statistics, but in this case a trade-off is made, because the angular resolution becomes worse. With two 32×32 DSSSDs at our disposal we decided to replace two out of four 16×16 DSSSDs from the 2006 setup, because the 32×32 detectors have a better angular resolution thanks to the reduced strip width (2 vs. 3 mm). Since alphas tend to be focused at small angles the reconstruction of their c. m. energy would generally suffer much more from a worsened angular resolution than would be the case for protons. For this reason it was decided to replace the small angle detectors and keep 16×16 detectors at large angles. As an added bonus the 32×32 detectors cover a larger solid area due to their superior size. They have a couple of drawbacks though. First their dead layer is about 630 nm silicon equivalent compared to 100 nm in the 16×16 detectors. Second they are extremely fragile[1].

In the 2006 experiment we ran for about 38 hours at 2.45 MeV and 6 hours at 4.9 MeV always with a beam intensity around 1 nA. Yet the number of $p + {}^{12}\mathrm{C}$ reactions observed was roughly the same in the two data sets, hence the important conclusion for this year's experiment was that we should run exclusively at 4.9 MeV since this choice would give us significantly higher statistics.

The sensitive structure of the silicon detectors that we employ in our experiment may essentially be characterized as a p-n junction in reverse bias. Any charged particle hitting the detector will produce electron-hole pairs along its path and eventually come to rest when all its energy has been exhausted. Thanks to the electric field over the junction the holes produced in its wake will be attracted to the p-doped side while the electrons will be swept to the n-side. The charges are collected by electrical contacts on the detector surface and give rise to an observable voltage pulse whose height is a direct measure of the energy of the ionizing particle. The average energy required to produce one electron-hole pair is largely independent of the velocity of the particle producing the radiation so the number of charges produced is proportional to the initial energy of the ionizing particle. Fluctuations are small because of the low energy required to produce an electron-hole pair (3.6 eV in silicon), hence the good energy resolution of semiconductor detectors. The charge produced by the ionizing radiation is typically collected within 1-10 ns. Despite the short collection time some charge carriers can be lost due to trapping and recombination. With sufficient bias voltage applied the detectors become fully depleted and the active region extends from one side of the detector to the other. However, thin surface dead layers due to electrical contacts and heavily doped layers of silicon cannot be avoided.

The four DSSSDs used in the 2006 experiment all measure 50×50 mm^2 and are 60 μm thick. Both sides of the detector are divided into 16 strips each 3.0 mm wide. Strips on one side are oriented perpendicular to those on the opposing side. On the front side the electric contacts only cover about 3% of the surface making the dead layer dominated by the inactive layer of heavily doped silicon which is only 100 nm thick. On the back side the electric contact covers the entire surface and the dead layer corresponds to about 630 nm silicon equivalent. A detailed description of the DSSSDs can be found in [Te04]. The back detectors we use are 1500 μm thick, also measure 50×50 mm^2 and have a dead layer of about 700 nm silicon equivalent on both sides.

[1]This proved fatal as one of the two 32×32 detectors cracked while mounting the setup and had to be re-replaced by a 16×16 detector.

Chapter 3

Monte Carlo simulation

When I first started working with simulations about three years ago I knew very little about them. Sure, I had heard about simulations before. People compare their experimental results to simulated ones all the time, but the whole concept of a simulation remained somewhat of a mystery to me. How could you possibly build a machine which is able to truthfully imitate the behaviour of a real physical system, which you do not yet fully understand? I also found it difficult to understand how you could simulate a microscopic system governed by the probabilistic laws of quantum mechanics. How could the simulation possibly predict when a certain unstable particle would decay? I was left with the impression that the program itself knew something that we did not know, which I found very strange.

Once I started working with simulations myself the mystery soon evaporated. As for my first question, "How can you build a machine which is able to truthfully imitate the behaviour of a real physical system that you don't fully understand?" the answer is "you can't". There is no more to the simulation than your own knowledge about the physical system whose behaviour you wish to simulate. If your understanding of the physical system is incorrect or incomplete the simulation will not imitate the behaviour of an identical system in the real world. It may be close to, and close enough for your purpose, but certainly not identical. As for my second question, "How can the simulation predict when an unstable particle will decay?" the answer again is "it can't". The computer does not know more than we do. In other words it is impossible to simulate the decay of a single unstable particle. What we can do is to simulate the decay of a large number of particles by generating random life times distributed according to an exponential distribution with the appropriate half-life, an approach known as the *Monte Carlo* method. Even though the simulation will be very different from the decay observed in the laboratory at the event-by-event level, it will be able to predict the observed decay spectrum of the entire sample. This very simple example illustrates the principle of Monte Carlo simulations, but does not make it clear why such simulations are needed. After all we could easily have predicted that the decay spectrum of the entire sample would be no different from the exponential distribution which was used to simulate the decay of each single particle. As we shall soon see the need for Monte Carlo simulations arises when the problems become more complicated.

In the context of experimental physics Monte Carlo simulations serve two purposes. Firstly they are used to optimize the setup in preparation for the experiment. Where should we place the detectors to maximize statistics? What is the energy range of the particles that we detect? How far can we raise the thresholds to eliminate noise without losing low-energy alphas? and so forth. Secondly they play a central role in the subsequent analysis because they allow a *quantitative* comparison of theory and data.

Simulations also serve as a very effiecient debugging tool. The program used to analyse the experimental data soon becomes very large and complicated. Errors are inevitably made and with many thousand lines of code the search for these errors becomes a time consuming business. By feeding the analysis program with simulated rather than real data errors become much easier to track down because we know what the output of the analysis should look like.

The fundamental element in any Monte Carlo simulation is an algorithm capable of generating a very long sequence of pseudo-random numbers distributed in the interval (0,1). The sequence is not truly random in that it is completely determined by a relatively small set of initial values, however it is uniformly distributed by any of several tests. My simulation makes use of the pseudo-random number generator RANLUX provided by CERNLIB, a large collection of general purpose libraries and modules in Fortran and C developed at CERN available at `http://cernlib.web.cern.ch/cernlib/`. Once equipped with a pseudo-random number generator it is straightforward to generate sequences of numbers x distributed according to any reasonably behaved probability function $f(x)$. Pseudo-random numbers are, as mentioned, not truly random in the sense that they are completely determined from a small set of initial values. This property is actually very useful to test the simulation for errors. If for instance a certain class of events (that correspond to certain input values from the sequence of random numbers) is causing segmentation faults in the simulation program, it would be difficult to track down the problem if the error did not show up next time you ran the simulation because the sequence of input numbers had changed.

3.1 The sequential model

Having introduced the general principles of Monte Carlo simulations I will now apply them to our specific case, namely the detection of charged particles produced in nuclear reactions induced by a few-MeV ^{3}He beam on targets made of ^{10}B, ^{11}B, and ^{7}Li. First I will discuss the simulation of the reaction itself. Later on I will explain how the detection system is added to the simulation to make it complete.

The simulation of the reaction rests on the concepts of the sequential model introduced in chapter 1, i. e. the reaction is modelled as sequence of two-body decays and any interaction between particles emitted at different stages of the decay is neglected. As discussed in chapter 1 reactions in each of the three targets lead to a multitude of possible reaction channels each mediated by a number of possible resonances. However, in the sequential picture all these reactions share a common structure which forms the skeleton of the simulation program. As sketched in figure 3.1 the reaction may be represented by a simple diagram where each line corresponds to a particle i_j, which if unstable eventually decays into two daughter particles $(i+1)_{2j-1}$ and $(i+1)_{2j}$.

Despite the general character of the problem I think a specific example will make it easier for the reader to understand (and for me to explain) the details of the simulations. Suppose we want to simulate the following channel[1]

$$
\begin{aligned}
{}^{10}\mathrm{B} + {}^{3}\mathrm{He} \rightarrow p + {}^{12}\mathrm{C}(9.64\ \mathrm{MeV}) & \\
\hookrightarrow\ \alpha_1 + {}^{8}\mathrm{Be}(\mathrm{g.s.}) & \\
\hookrightarrow\ \alpha_2 + \alpha_3 &
\end{aligned}
$$

[1]Notice how the general reaction diagram accomodates this particular channel: $p \rightarrow 1_1$, $^{12}\mathrm{C} \rightarrow 1_2$, $\alpha_1 \rightarrow 2_3$, $^{8}\mathrm{Be} \rightarrow 2_4$, $\alpha_2 \rightarrow 3_7$, and $\alpha_3 \rightarrow 3_8$.

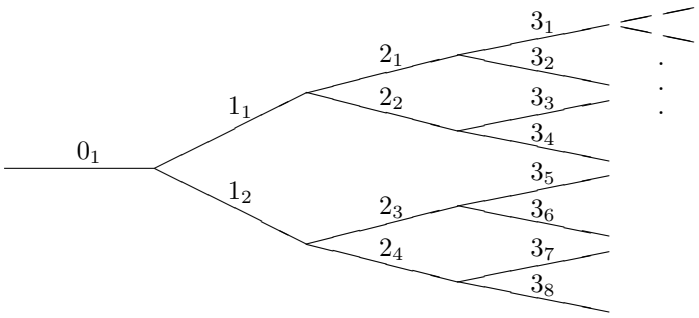

Figure 3.1: The sequential model

To make it simple we neglect the width of the intermediate resonances, ^{12}C(9.64 MeV) and ^{8}Be(g.s.), which is a perfectly legitimate approximation for the latter, but not quite for the former whose width is 34 keV. The first step of the reaction is most easily described in the center of mass frame. With the ^{12}C excitation energy fixed at 9.64 MeV the kinetic energy available to the proton and the ^{12}C nucleus can easily be calculated from the chosen beam energy and the known nuclear masses. As in any other reaction leading to a two-body final state the two fragments leave the reaction site back-to-back with energies uniquely determined by energy and momentum conservation. A classical calculation shows that the energy is divided inversly proportional to the ratio of masses, i. e. 1:12 in favour of the proton. However, since protons with energies up to 20 MeV are observed in the experiment the simulation is entirely based on relativistic kinematics. The proton angular distrubution depends on the dynamics of the reaction. In a direct reaction the protons would preferentially be emitted in the forward direction, while isotropic emission would be expected if the reactions proceeds through a compound resonance in ^{13}N. Lacking any arguments that would favour one reaction model over the other we assume the protons to be emitted isotropically because it is the simplest possible angular distribution. Isotropic emission is generally assumed when no arguments based on the dynamics of the reaction or conservation of angular momentum suggest a different distribution. Before proceeding to the second stage of the reaction we select a unit vector from a sample of vectors uniformly distributed over the unit sphere, which represents the direction of motion of the proton in the c. m. frame[2].

The subsequent decay of the ^{12}C(9.64 MeV) resonance is most easily treated in the rest frame of the decaying nucleus. With both decay products having a fixed mass their kinetic energy is, as before, uniquely determined by energy and momentum conservation. The 4-momenta of the alpha particle and ^{8}Be nucleus are transformed to the c. m. frame using the well-known Lorentz transformation rules[3]. Notice that the relative velocity of the two inertial frames is simply the velocity of the decaying ^{12}C nucleus as determined in the first stage of the reaction.

It should come as no surprise that the last stage of the reaction, the break-up of the ^{8}Be ground state into two alphas, is treated in a very similar fashion. Since the ^{8}Be ground state posses no spin it has, so to speak, no directional memory. Therefore no angular correlations exist between the alpha particle emitted in the decay of ^{12}C and

[2]In polar coordinates isotropic emission corresponds to a uniformly distributed azimuthal angle ϕ while the polar angle θ is distributed according to $f(\theta) \propto \sin\theta$.

[3]The transformation formulas becomes quite complicated when the relative motion of the inertial frames is not parallel to one of the cartesian axis, but the transformation may still be written in terms of 4×4 matrix to be multiplied by the 4-momenta.

the two alpha particles from the break-up of ^{8}Be(g.s.). Whenever the decay proceeds through the broad 2^+ state in ^{8}Be angular correlations will usually be present. The exact form of the correlation depends on the spin of the initial resonance in ^{12}C and can be derived from the quantum mechanical theory of angular momentum as discussed in [Bi53].

It is clear that the approach described in this specific example lends itself to the description of any chain of two-body decays. We merely have to change the nuclear masses and define new angular correlation functions appropriate to the new problem. Gamma decays can easily be accomodated within the simulation by setting the mass of the emitted photon equal to zero.

3.2 Broad resonances, interference effects, and more

Before proceeding to the discussion of the detection system a few complications to this simple reaction model need to be mentioned. Whenever the resonances involved in the reaction become wide compared to our experimental resolution of 15-20 keV (cf. chapter 4) they cannot be treated as particles of fixed mass. In most cases the shape of the resonance can be described by a simple Breit-Wigner profile and the particle mass, and hence the energy available to its decay products, depends on the energy at which the resonance is populated. This effect is easily included in the simulation by the Monte Carlo method: Each time the simulation is repeated (for typical applications a million times or more) we select a new excitation energy from a large sample of values distributed according to a Breit-Wigner distribution with the appropriate width and resonance energy.

On a few occasions the resonances become so wide that the shape is not well-described by a simple Breit-Wigner profile. This happens to be the case for the broad 2^+ state in ^{8}Be and also for the unbound ground state of ^{5}Li.

Due to the short range of the nuclear force a reaction can only occur if two nuclei are brought very close together. Thus space can be divided into two regions. Whenever the nuclei are separated by a distance larger than some fixed radius R, usually taken as the sum of the nuclear radii, nuclear forces are assumed to be negligible. The only forces acting between the nuclei is the Coulomb repulsion and their relative motion is described in terms of well-known Coulomb wave functions. Inside the sphere of radius R nuclear forces take part in the game and things become complicated. The probability to form a certain resonance in a reaction between two nuclei (or, conversly, the decay width of the resonance) will factorize in three contributions, the phase space factor, the probability to penetrate the Coulomb and centrifugal barrier, and the probability to form the resonance once inside the barrier. The first two are lumped together in what is known as the *penetrability* and its value only depends on the choice of radius R as well as the mass, charge, energy, and angular momenta of the colliding nuclei. The probability to form the resonance once inside the barrier depends on the details of the nuclear force. In the case of a single isolated state its profile is well-described by a Breit-Wigner distribution. Notice that the properties of the nuclear force only enters the calculation of the penetrability through the choice of radius R. The remaining parameters are all known. This property of the penetrability explains its usefulness. It separates the well-understood part of the problem from the part that depends critically on the not-so-well-understood nature of the nuclear force. If the resonance is fairly narrow the penetrability will be constant to a good approximation over the resonance region, but in the case of a very wide resonance the energy dependence of the penetrability can no longer be neglected. Since the probability to tunnel through the Coulomb and centrifugal barrier

increases with energy the resonance profile will become assymetric with a pronounced high-energy shoulder. The multiplication of a decreasing Breit-Wigner profile[4], with an increasing penetrability may even result in the appearance of ghost states as illustrated in figure 3.2 as is the case for the famous Hoyle state in ^{12}C [Ba62].

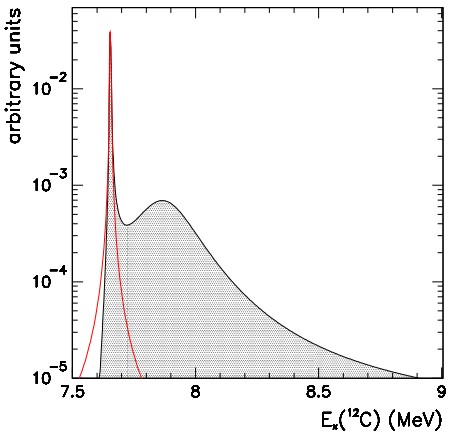

Figure 3.2: The profile of the Hoyle state when the effects of penetrability are included (shaded grey) with the standard Breit-Wigner shape superimposed (red).

When broad resonances overlap their profile cannot be described as a sum of two Breit-Wigner profiles and the more general R-matrix theory [La58] is used to parametrize the nuclear leves. Interference effects may occur between states of same spin-parity. This effect follows from basic quantum mechanics. Imagine a nuclear state ψ_i of definite spin-parity which can decay to a number of states in the daughter nucleus. If two of these states ψ_1 and ψ_2 happen to have identical spin-parity it is possible for the initial state to decay to a superposition of the two $\alpha\psi_1 + \beta\psi_2$. The decay to a mixture of two states with different spin-parity is not possible because the nuclear Hamiltonian is generally assumed to be rotationally invariant making the angular momentum a good quantum number. The relative contribution of the two states, α and β, depends on the details of the decay, but are not relevant for our considerations. The important point is that the daughter nucleus is populated in a superposition of two states with the same spin-parity but different energies. If this mixed state subsequently decays to a final state ψ_f under the action of some interaction Hamiltonian $H_{\rm int}$ the decay-rate has to be calculated by the standard methods of quantum mechanics

$$\begin{aligned}\Gamma &\sim |\langle\alpha\psi_1 + \beta\psi_2|H_{\rm int}|\psi_f\rangle|^2 \\ &= |\alpha|^2|\langle\psi_1|H_{\rm int}|\psi_f\rangle|^2 + |\beta|^2|\langle\psi_2|H_{\rm int}|\psi_f\rangle|^2 \\ &\quad + \alpha^*\beta\langle\psi_1|H_{\rm int}|\psi_f\rangle\langle\psi_2|H_{\rm int}|\psi_f\rangle^* + \alpha\beta^*\langle\psi_1|H_{\rm int}|\psi_f\rangle^*\langle\psi_2|H_{\rm int}|\psi_f\rangle\end{aligned}$$

The last two terms will give rise to interference effects in the observed spectrum.

Finally I would like to point out that interference effects may be expected between the alpha particles emitted in the ^{10}B(^{3}He, $p\alpha\alpha\alpha$) reaction. Especially when the reaction proceeds through the very short-lived 2^+ state in ^{8}Be with all three alpha particles emitted at nearly the same location in space-time. Being identical bosons the 3α wave function has to be made symmetric and this leads to interference between the alphas. Presently this effect is not accounted for in the simulation, but will eventually be included following the prescription given in [Fy03] where the effects of interference among the alphas were observed in the decay of the 12.71 MeV resonance in ^{12}C.

[4]The resonance profile may still be written as $\frac{\Gamma}{2\pi}\frac{1}{(E-E_0)+(\Gamma/2)}$ however the width Γ is no longer constant but proportional to the penetrability and hence energy-dependent.

3.3 Detecting the particles

With the simulation of the reaction now working all that remains is to incorporate the detection system. The idea is basically to mimic the behaviour of the experimental setup as closely as possible using the output from the simulation of the reaction as the input for our simulated detection system.

First we have to figure out if the particle emitted actually hits any of our detectors. If so, which front and back strips will it be hitting? This is a simple geometrical problem, but obviously requires knowledge of the measures of the real setup. As discussed in chapter 4 the relative position of the detectors are easily measured with a ruler, while their exact position relative to the beam spot can be obtained from the data by requiring momentum conservation in 4-coincidence events. The next step will be to calculate the energy deposited by the particle in the dead layer and the active region of the DSSSD, which is accomplished using tabulated values of the stopping power and range of ions in solids [Zi03]. Knowledge of dead layer and detector thickness is obviously required to perform these calculations. If the particle is not brought to rest in the DSSSD its energy deposit in the back detector must also be calculated taking into account the dead layers on the back side of the DSSSD and on the front of the back detector. If two particles happen to hit the same strip in coincidence their energy is added together (times of flight vary between 1 and 10 ns, hence the delay between two coincident pulses will be small compared to the time resolution of the electronics which only registers the combined signal). The resolution of the detector and the electronics system is taken into account by adding a gaussian variable with σ around 15-20 keV (depending on the detector). In addition an appropriate correction is made for the pulse height defect (cf. chapter 4) of non-alpha particles because the calibration was performed with alpha particles.

If an energy signal above the trigger threshold is recorded in any of the triggering channels the event is accepted and all other energy signals induced in the detectors by this particular event are saved if above the ADC threshold. Obviously trigger and ADC threshold must be measured in the real experiment to make this selection possible.

A few more details will eventually be added to the simulation of the detection system, but the basic ingredients have now all been presented. The output of the simulation is saved to a file whose structure is almost identical to the real data such that it can serve as an input to the analysis program used for the real data. The only difference between the structures of simulated and real data files is that the former contain some extra information compared to the latter that makes it possible to test the analysis program. For instance the simulation could be used to test how good the analysis algorithm is at identifying summing events.

By now it should be clear why Monte Carlo simulations are indispensable tools in the analysis of many physics experiments. Without simulations it would be very difficult to make a quantitative comparison of data and theory. Having said this one must always keep in mind that the output of the simulations ultimately results from the knowledge that was used to construct it. Consequently we should always be able to explain, at least at the qualitative level, any predictions made by our simulation. If we fail in doing so, how do we know that the simulation program is not making an error. And even if it is not, can we still claim to have *understood* the results of the experiment?

Chapter 4

Analysis

As previously mentioned the 2006 data contains comparable amounts of statistics at 2.45 and 4.9 MeV. The existence of two data sets has made it possible to cross-check any results and generally I have always found good agreement between the two data sets. Some observables, such as the proton angular distribution, we expect to depend on the beam energy, while others, e. g. the decay mechanism of any intermediate resonance, should not. The results I will be presenting here are drawn from both data sets.

4.1 Calibration and detector response

The detectors were calibrated using the standard radioactive sources ^{148}Gd and ^{241}Am. The former emits alphas with an energy of 3183 keV, while the latter gives rise to three alpha lines at 5486, 5443, and 5388 keV whose relative intensities are 85.2%, 12.8%, and 1.4% respectively [Fi96]. The energy calibration is performed at pressures below 1×10^{-5} mbar to avoid energy loss in air.

Since the source is placed at a distance to the detector comparable to the dimensions of the detector itself the incident angle will vary considerably over the surface of the detector. Consequently the alpha particles will traverse dead layers of varying thickness leading to a shift and a broadening of the alpha lines. As discussed in chapter 2 the front side dead layer of the 16×16 DSSSDs is only 100 nm thick and therefore the line broadening due to variations in the incident angle over over each strip will be very small. A SRIM calculations predicts an energy loss of only 19 keV when 3183 keV alphas traverse 100 nm of silicon, while 5486 keV alphas lose slightly less, 14 keV. The energy shift in each strip is calculated as the average of all 16 single-pixel shifts weighted by the solid angle of each pixel. However, in order to calculate the solid angle covered by each pixel as well as its effective dead layer one must know the position and orientation of the detector relative to the source. In principle a precise measurement of the geometry could be made to the required accuracy by using a standard ruler, but the fragility of the detectors makes such a measurement impractical. A much more convenient and accurate method consists in fitting the intensity distribution expected from a point source to the distribution actually observed on the DSSSD with three parameters defining the detector-source geometry as free variables. Figure 4.1 shows the hit distribution from a point source somewhat off center together with a typical single-strip calibration spectrum.

The observed line width in the single-strip spectrum represents the combined effect of our experimental resolution, the variations in dead layer thickness along the strip, and the line broadening expected from the implantation depth profile of the radioactive material in the source. The experimental resolution has itself many contributing factors both

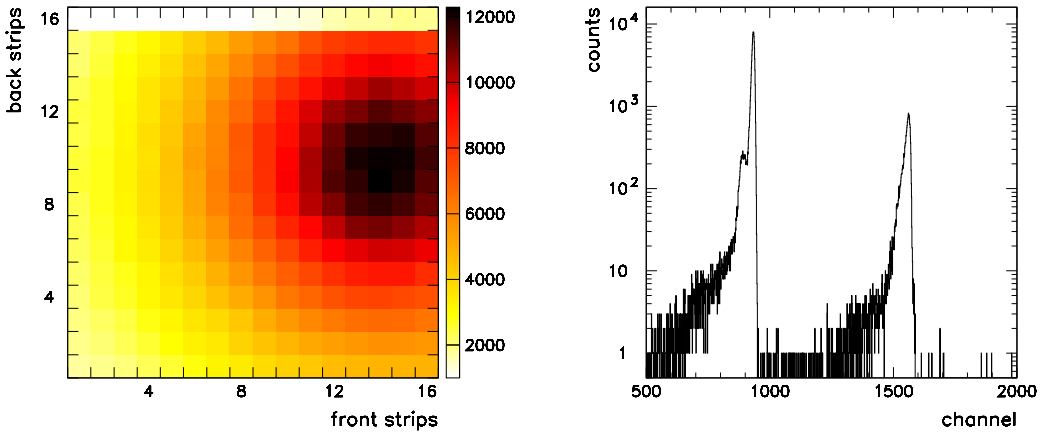

Figure 4.1: Hit distribution from a point source somewhat off center (left) and a typical single-strip calibration spectrum (right). The three ^{241}Am alpha lines are not discernable by eye inspection due to the experimental resolution.

related to physical mechanism by which charge is produced and collected in the detector and the subsequent handling of the electronic signal. Both peaks have a low-energy tail which represents the effect of incomplete charge collection due to recombination and trapping of charge carriers in the silicon. The ^{148}Gd peak displays an additional bump located about 40 channels below the main peak. We think the presence of this bump could be accounted for by the additional energy loss experienced by alphas hitting the aluminium contacts that cover about 3% of the detector surface. However, 40 channels corresponds (for this particular strip) to an energy difference of about 150 keV which requires electrodes 900 nm thick, much more than the 200 nm stated by the producer. No clearly discernable bump is observed in relation to the ^{241}Am peak because the amount of statistics is much reduced. Forgetting the bump for a moment the peak profile turns out to be nicely described by a Gaussian convoluted through two low-energy exponential tails. A two-dimensional plot showing corresponding back and front strip energy signals holds more information than the one-dimensional spectrum, especially on the difference between front and back strip behaviour reflecting the different design of the two sides of the detector and the fact that electrones and holes do not behave merely as identical charge carriers of opposite sign. In the near future I intend to carry out a careful study of the detector response based on the alpha source measurements and reaction data collected in the most recent CMAM experiment.

When calibrating the unsegmented silicon pads we place a collimator 1 cm in diameter in front of the detector to reduce the spread in incident alpha angles. The dead layer of the pads consists of 300 nm aluminum conduct and 400 nm p-doped silicon. Using SRIM tables the average energy energy loss of 3183 keV alphas is found to be 143 keV, while 5486 keV alphas lose somewhat less, 101 keV.

It is well known that the ionization energy in semiconductors, i. e. the energy required to form a single electron-hole pair, has a weak dependence on the charge and mass of the ionizing particle. Protons and alpha particles of the same energy will produce slightly different amounts of electron-hole pairs and hence give rise to electric pulses of slightly different height. The ratio of the two pulse heights is called the *pulse height defect* and

it turns out that this ratio is largely independent of the pulse height, making a separate calibration of the detectors with proton sources unnecessary, since proton energies just have to be divided by the pulse height defect to correct the error induced by the small difference in ionization energy. I use the value 0.989 quoted in [Le86] both for protons and deuterons.

Since the alpha sources do not cover the full energy range observed in the experiment (0-10 MeV in the DSSSDs and 0-20 MeV in the back detectors) the calibration becomes less accurate at high energies. To overcome this problem an internal calibration of the back detectors was done based on the known level energies of three narrow and thus easily discernable states in ^{12}C at 9.64, 12.71 and 16.11 MeV excitation energy[1].

4.2 Matching of front and back strips

With the calibrations sorted out we can move on to the analysis of the real data. Matching front and back strip energy signals constitutes the first point of the agenda. In the simplest of all scenarios there is a single energy signal from each side of the DSSSD and the matching is straightforward. If the same detector is hit by more than one particle we must compare energies to figure out which front and back strips to match. How close do the front and back energies need to be before we can say that they are equal? This obviously dependes on the resolution of our detector. In single-particle events a restriction on the energy difference between front and back signals is useful to cut out noise. If a particle happens to hit a dead strip, i. e. one which is not working due to a broken electrical contact, one of the two energy signals will be missing and a front-back matching cannot be made. A similar effect is seen if a low-energy particle produces a signal which is below the ADC threshold in one strip, but survives in the other. Charge sharing between adjacent strips and summing (two particles hit the same strip in coincidence) is responsible for a sub-class of events where the matching of front and back strips becomes especially difficult. Currently my analysis includes a routine to identify summing events, while the effects of charge sharing have yet to be included.

The line width observed in the calibration spectra provides an estimate of the experimental resolution, but since the contribution due to the implantation depth profile of the radioactive material in the source is unknown, it merely provides an upper limit on the resolution. To get an actual number we can look at the difference between front and back strip energies in the real data. Assuming that front and back strip signals may be treated as independent stochastic variables both distributed according to a Gaussian response function of standard deviation σ we expect the *difference* between front and back strip energies also to be distributed according to a Gaussian profile whose standard deviation is $\sqrt{2}\sigma$ (this is easily verified). As was evident from the calibration spectrum on figure 4.1 the response function is not quite Gaussian in that it has an exponential tail, whose effect however must be small and can be accounted for if needed. The assumption of independence is more problematic. Since the front and back signals arise from the collection of charges (electrons and holes, respectively) produced in equal numbers by the same ionizing particle correlations must be expected. It is true that fluctuations in the energy signal are dominated by the process of charge collection and the subsequent handling of the electronic signal, not the stochastic nature of charge production, but the charge collection is itself to some extent dependent on the charge production process in that the collection efficiency depends on the distance the charges have to travel to reach

[1] To be honest the calibrations of the back detectors had not been performed carefully enough and were useless from the beginning, so an internal calibration had been necessary in all cases.

the electrode. Therefore front-back correlations could even be present in the process of charge collection. Anyhow, assuming independece I obtain four σ-values (one for each DSSSD) all in the range 15-20 keV. In all four detectors σ is observed to decrease by 1-2 keV over the energy range of the detector (0-10 MeV). Figure 4.2 shows what the front-back energy difference looks like in DSSSD 3 in the energy range 3-4 MeV.

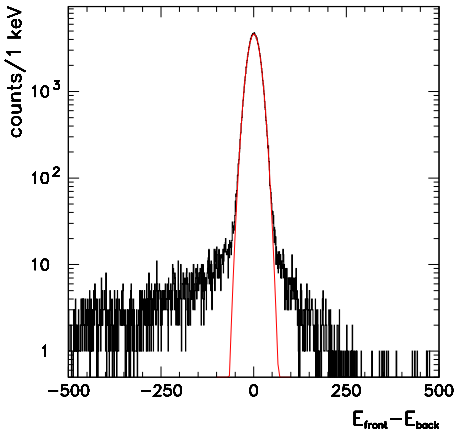

Figure 4.2: Front-back energy difference in DSSSD 3 in the energy range 3-4 MeV from real data. Only events with exactly one front and one back strip signal are included in the plot.

Indepedent or not, the front-back energy difference is seen to have a Gaussian distribution. The standard deviation can be used to define what it means for two energy signals to be equal. In my analysis I require the difference to be less than three standard deviations.

4.3 Particle identification

Particles that penetrate into the silicon pad mounted behind the DSSSD can be identified in two-dimensional plots with the DSSSD energy ΔE along one axis and the back detector energy E along the other axis. This is because the energy loss per path length $\frac{\mathrm{d}E}{\mathrm{d}x}$ is a function of the charge and velocity of the ionizing particle. The ΔE-E plot for DSSSD 2 is shown in figure 4.3. Three banana-shaped regions of high intensity are clearly visible in the plot. From top to bottom they correspond to alphas, deuterons, and protons. Particles with more than 5 MeV that are stopped in the DSSSD can also safely be assumed to be alphas.

At 15.7 MeV the proton banana is observed to "turn around" because the protons start punching through the telescopes. Unfortunately the finite energy resolution of the detectors prevents a clean separation of the punch through protons. At even higher proton energies the DSSSD signal falls below the threshold and the protons are lost.

If a detector is hit by more than one particle and one penetrates into the back detector we have to figure out which one it was. In most cases one of the DSSSD signals can be matched with the energy measured in the back detector to yield a point in the ΔE-E plot inside one of the bananas, while the remaining hits in the DSSSD yield points outside the bananas when matched with the back detector energy.

In principle all statistics should be confined to the bananas in the ΔE-E plot and this is indeed the case for the vast majority of all hits. However a relatively small number fall outside the bananas. The existence of these spurious hits is only partly understood at the moment. The exponential tails of the response function could explain some of them. Others, we think, are due to random coincidences with positrons from beta-

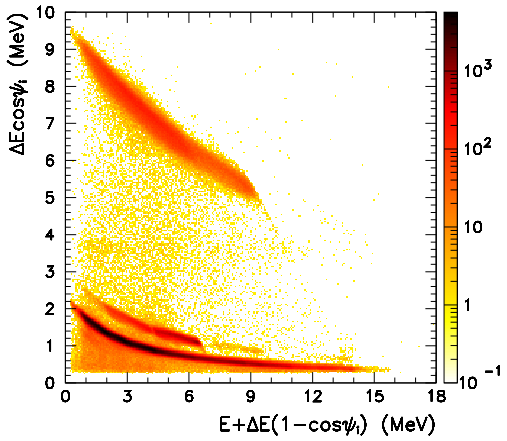

Figure 4.3: ΔE-E plot for DSSSD 2 with first order corrections for variations in DSSSD thickness due to the incident angle ψ_i. The three banana shaped regions are (in descending order) alphas, deuterons, and protons.

decays of ^{11}C produced in the reactions $^3\mathrm{He} + {}^{10}\mathrm{B} \rightarrow d + {}^{11}\mathrm{C}$ and $^3\mathrm{He} + {}^{12}\mathrm{C} \rightarrow \alpha + {}^{11}\mathrm{C}$ (the existence of events which contain nothing but a single energy signal from the back detector supports this hypothesis). Others still can be explained as coincidence events where the penetrating particle hits a dead strip and consequently fails to survive the front-back strip matching, or if the penetrating particle is a highly energetic proton its energy deposit in the DSSSD may be so small that it falls below the ADC thresholds.

Recently I have started to look at the timing signals which should provide further clues to the origin of the hits observed outside the bananas. I anticipate that a satisfactory understanding of the effects will soon be reached.

4.4 Geometry considerations

The relative position and orientation of the detectors and the target is measured before the setup is placed inside the chamber, but the exact location of the reaction site is determined from the data itself by requiring momentum conservation in all 4-coincidence events. Figure 4.4 shows how the single particle momenta add up to the initial ^{3}He momentum along the beam axis (z) and the total transverse momentum is zero (x and y) when the correct geometry is chosen (black). The red histogram shows what happens if the reaction site is assumed to be located just 1 mm further down stream than the actual position. The accuracy of this method is better than 0.5 mm. While very sensitive to the geometry this method is quite *in*sensitive to errors in the energy. Suppose a particle of mass m and energy E is measured to have the energy $E + \Delta E$ due to an erroneous calibration or simply because the particle lost some of its energy in the detector dead layer. It is easy to show that if ΔE is small compared to E the error made when calculating the momentum will be $\Delta p \simeq 22$ MeV/c$\sqrt{mE}\frac{\Delta E}{E}$ with E in MeV and m in units of the proton mass. If for instance the calibration is 25 keV off the momemtum of a 2 MeV alpha will only be wrong by 0.8 MeV/c, while the shift caused by moving the reaction site only 1 mm too far down stream is already 6 MeV/c.

With the geometry and particle identification sorted out we are now able to calculate the energy lost by each particle in traversing the detector dead layers whose effective thickness depend on the incident angle. Particles that could not be identified because they were stopped in the DSSSD are assumed to be alphas in these calculations. Particles also lose energy in the target itself, but the amount varies depending on the depth to

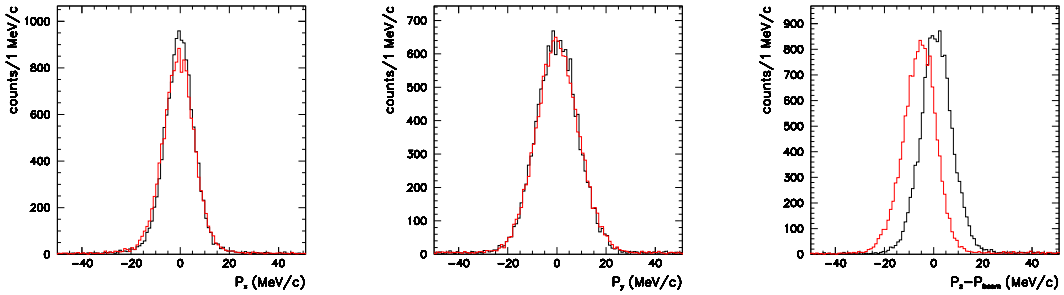

Figure 4.4: Total final state momentum in 4-coincidence events assuming the correct geometry (black) and with the reaction site located just 1 mm further down stream than the actual position (red).

which the beam particle penetrates before colliding with a target nucleus. Since the targets are very thin (18.9μg/cm^2 of ^{10}B and 3μg/cm^2 of ^{12}C corresponding to 80 and 13 nm, respectively) the energy lost by the beam particle is negligible and its reaction cross section hence constant implying a exponentially decreasing depth profile. However the interaction length is so long compared to the target thickness that the depth profile is essentially flat, so on average reactions take place in the center of the ^{10}B target. Note however that the presence of the carbon backing makes things slightly more complicated.

Finally we transform all laboratory energies and angles to the c. m. frame where the physics is most easily interpreted. In 3 and 4-coincidence events it is often possible to determine the mass of unidentified particles (i. e. particles that were stopped in the DSSSD) by exploiting energy and momentum conservation. If such an unidentified particle turns out to be a proton or a deuteron (hence not an alpha as originally assumed) energy loss corrections and the transformation to the c. m. frame has to be re-done with the correct mass and before doing so one must correct for the pulse height defect too.

4.5 Kinematic curves

The initial stage of the analysis is finally completed. It is time to do physics. In any two-body reaction the c. m. energy of each fragment is uniquely determined by energy and momentum conservation. When transformed to the laboratory system the energy E depends on the angle of emission θ. The correspondance between E and θ is one-two-one if the fragment has a c. m. speed which is larger than the boost velocity. In the opposite case two energies are possible for each value of θ. In both cases the relation between E and θ can be represented by a continous curve, known as the kinematical curve, in a two-dimensional plot with E along one axis and θ along the other.

Figure 4.5 displays the experimental data separated into protons, deuterons, alphas and unidentified particles. These plots offer a great starting point for our analysis because they can tell us which nuclei are present in the target and what two-body reactions are induced by the beam on these targets. Each ^{12}C state populated in the $p + ^{12}$C channel is represented by a kinematic curve in the proton plot. The higher the excitation energy the lower the curve. The $p + ^{14}$N channel from reactions on the carbon backing produces a whole spectrum of kinematic curves which can be distinguished from the carbon curves by their slightly smaller gradient. The two intense lines in the deuteron plot represent the ground state and the 1$^{\text{st}}$ excited state population in the $d + ^{11}$C channel, while the two high-lying low-intensity curves represent the population of the ground state and first

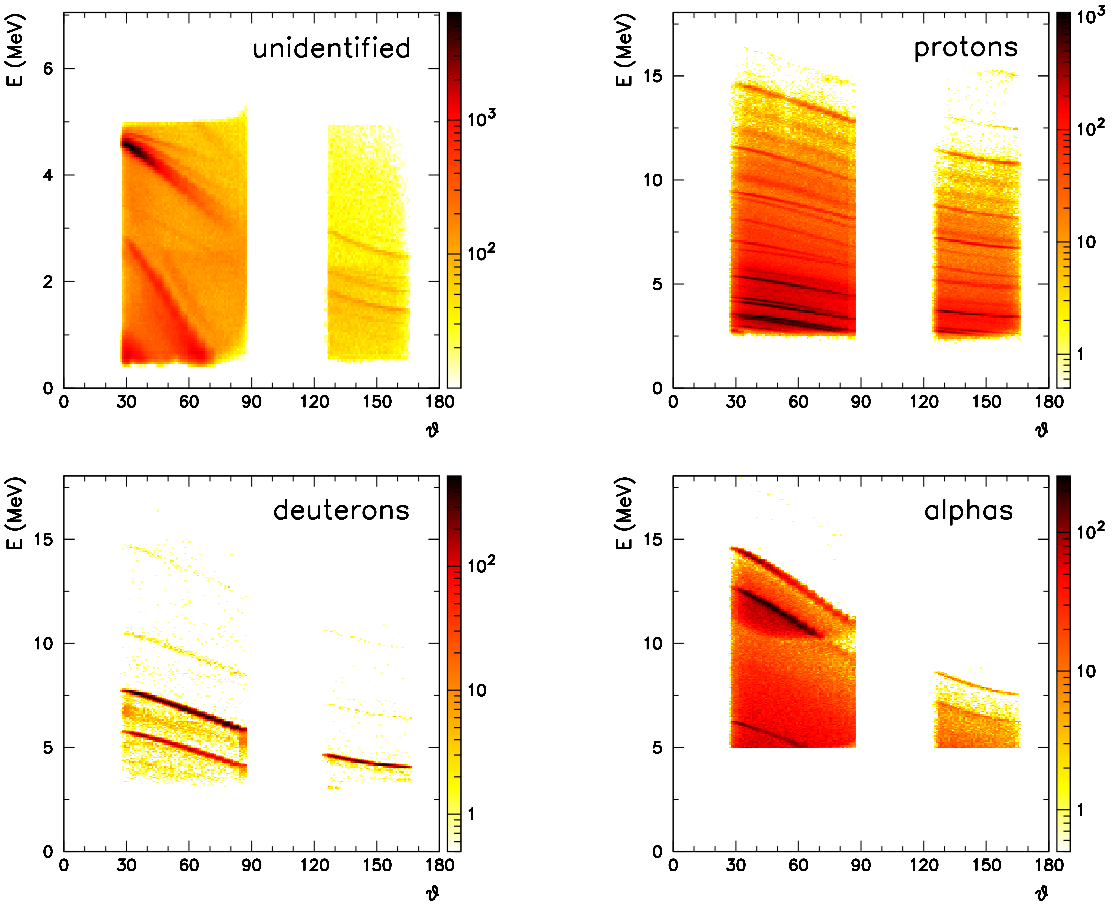

Figure 4.5: Energy vs. angle, all particles detected in DSSSD 2 and 3 are included in the plots.

excited state in ^{12}C in the reactions on the ^{11}B impurities in the target. In the alpha plot we clearly see the population of the ground state and 2.36 MeV state in ^{9}B as the two highest-lying curves. The $\alpha + {}^{11}$C(g.s.) channel from reactions on the carbon backing can be seen as the low-lying curve. The last plot with all the unidentified particles is dominated by Rutherford scattering. A close inspection reveals that several components contribute to the elastic scattering of beam particles. Most notably boron and carbon, but also aluminum and copper are seen to contribute.

4.6 Multi-particle detection

Figure 4.6 shows the ^{12}C excitation spectrum with increasing mutiplicity. When all protons are included without regard to the event multiplicity both ^{12}C and ^{14}N states appear in the spectrum. If we require at least one particle to have been observed in coincidence with the proton the amount of statistics drops, but the ^{14}N are still visible due to $p + {}^{14}$N coincidences. However, when we go one step further up the multiplicity ladder we see that all ^{14}N peaks vanish as expected. The 15.11 MeV state in ^{12}C also disappears because it mainly decays by gamma emission to the ground state.

As was demonstrated by Waggoner in 1966 much can learned from $p+\alpha$ coincidences about the channels that contribute to the ^{10}B(^{3}He, $p\alpha\alpha\alpha$) reaction. However, a full kinematics measurement where three or all four final state particles are detected allow

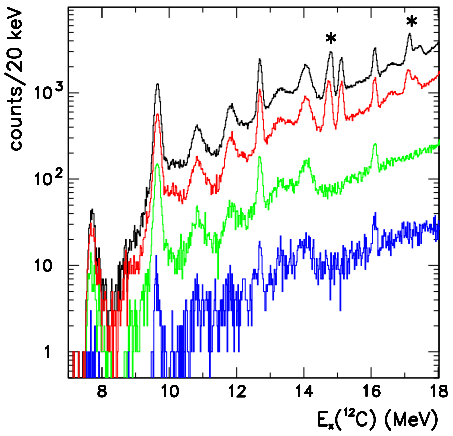

Figure 4.6: ^{12}C excitation spectra with conditions on the multiplcity. The black curve is obtained by including all protons, the red curve requires at least one hit in coincidence, the green curve two, and the blue three. ^{14}N peaks are indicated with an $*$.

us to answer many more questions. Therefore it is unfortunate that the number of 3 and 4-coincidence events is so limited in the 2006 data.

False 4-particle events due to random coincidences can be identified and elimininated by checking energy and momentum conservation. In figure 4.7 the total energy of the four particles is plotted along the first axis while the momentum loss $\Delta P = |\sum_i \vec{P}_i - \vec{P}_{\text{beam}}|$ is plotted along the second axis. Most 4-particle events are true coincidences and lie inside the box. False 3-particle events can also be identified, but our ability do distinguish

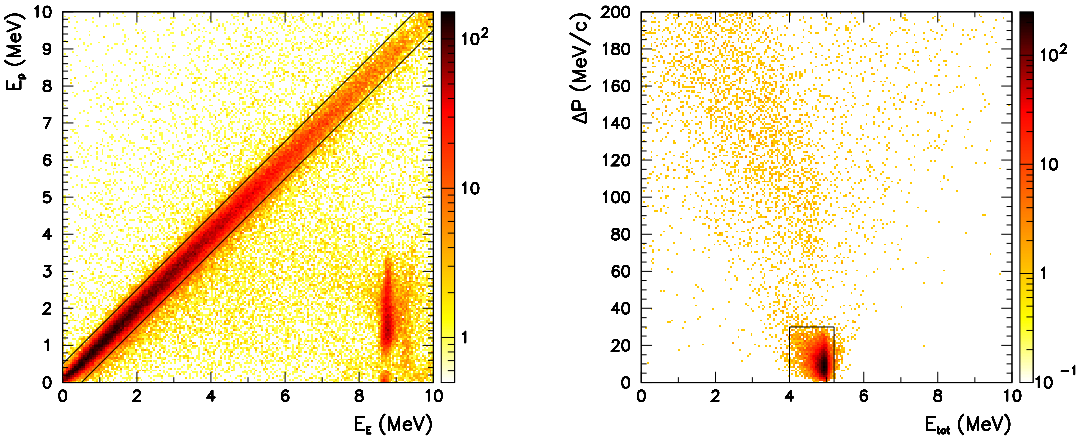

Figure 4.7: Cuts imposed on 3 and 4-coincidence events (left and right, respectively).

between true and false events is not as good as for 4-coincidences. Having measured the energy and direction of three particles we can compute the energy of the fourth missing particle using either energy or momentum conservation. If the two calculations agree to some defined accuracy (500 keV in my case) we accept the event as a true 3-coincidence. When using momentum conservation to calculate the energy of the fourth missing particle an assumption must be made regarding its mass. This is straightforward if the proton has been identified among the three observed particles, because then the fourth particle has to be an alpha if we are dealing with a true coincidence. Things become slightly more involved if the proton has not been identified among the three

observed particles. Then we must try out every possibility and chose the one that meets the conditions imposed on the 3 and 4-coincidence events as explained above. Using simulations one can test how efficient this method is at "digging up" protons from below the identification threshold.

4.7 An overview of the ^{10}B(^{3}He, $p\alpha\alpha\alpha$) reaction

Referring to the work by Waggoner et al. our hypothesis is that the ^{10}B(^{3}He, $p\alpha\alpha\alpha$) reaction can be described as a sequential process with contributions from three main channels, $p+^{12}$C, $\alpha+^9$B, and ^{5}Li$+^8$Be. Waggoner's conclusions were merely qualitative ones. He did definitely see evidence for the first two channels, while nothing could be said with certainty regarding the third channel. As we shall see in a moment the 3 and 4-coincidence events allow us to go much further than Waggoner. By comparing the results of simulations to our data we can test the sequential model on a *quantitative* level and determine if the ^{10}B(^{3}He, $p\alpha\alpha\alpha$) reaction can be entirely understood in terms of the three main channels $p + ^{12}$C, $\alpha + ^9$B, and ^{5}Li $+ ^8$Be, or if some other entirely different mechanism makes an important contribution to the reaction.

In any 3 and 4-coincidence event we can check if the ^{8}Be ground state was formed as an intermediate resonance in the reaction by the invariant mass technique. If the relative energy of any two alphas correspond to the ground state energy in ^{8}Be we assume that the ^{8}Be ground state was indeed formed as an intermediate resonance in the reaction and that these two alphas come from its break-up. The narrow width of the ^{8}Be ground state is the reason for the feasibility of this method. When the energy available to the three alphas becomes small, as is the case in the decay of the Hoyle state, the identification becomes problematic.

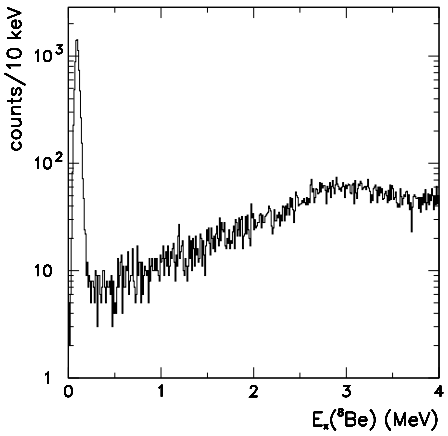

Figure 4.8: ^{8}Be excitation spectrum based on 4-coincidence events (all three possible alpha-pairs are included in the plot).

If ^{8}Be(g.s.) is indeed formed in the reaction we are effectively dealing with a three-body final state, thus all the information encoded in the particle energies can be displayed in a two-dimensional plot with the proton c. m. energy along the first axis and the alpha energy along the second axis (here we obviously choose the alpha particle that is not from the break-up of ^{8}Be). The $p + ^{12}$C channel will show up as vertical lines of increased intensity, the proton energy decreasing with increasing ^{12}C excitation energy, while the $\alpha+^9$B channel will be seen as horizontal bands (figure 4.9). The third channel ^{5}Li $+ ^8$Be(g.s.) should if present be seen as diagonal bands.

When ^{9}B does not decay via the ^{8}Be ground state there is no way for us to tell,

event-by-event, which alpha was the first to be emitted. We can pick one at random or we can chose the one with the smallest angle of emission in the c. m. frame, since if we believe (which we tend to do) that the initial two-body reaction $^3\mathrm{He} + {}^{10}\mathrm{B} \rightarrow \alpha + {}^9\mathrm{B}$ is a direct reaction (one-neutron pick-up) we would expect the alpha to be focused in the forward direction. Obviously we are bound to make the wrong choice on many occasions. However, since correctly identified alphas will be confined to certain narrow horizontal bands while wrongly identified alphas will be distributed randomly on the plot, horizontal bands of increased intensity should still be expected to show up in the plot (figure 4.10).

If the reaction is found to proceed through the ground state of $^8\mathrm{Be}$ we look for $^5\mathrm{Li}$ resonances in the proton-alpha relative energy spectrum (figure 4.12). If not we pick one alpha at random (in this case we do not expect the alpha to be emitted in any preferred direction), compute its relative energy to the proton, compute the relative energy of the remaining two alphas, and plot these two energies against each other and look for regions of increased intensity (figure 4.11).

While channels proceeding through narrow states are easily identified, the contribution from very broad intermediate resonances is difficult to separate from the background caused by other channels and wrongly identified alphas. The most extreme example would be the $^5\mathrm{Li}(1/2^-) + {}^8\mathrm{Be}(2^+)$ channel where the widths are about 6.6 and 1.5 MeV, respectively. I think the only way to see the contribution of this channel would be a comparison of the data to an extensive simulation that includes all other channels known to contribute to the $^{10}\mathrm{B}(^3\mathrm{He}, p\alpha\alpha\alpha)$ reaction. If the data shows any excess compared to the simulation in the region where this channel is expected to contribute it would be evidence of its presence (assuming that the simulation gives a faithfull reproduction of all other channels).

	channel	^{8}Be	resonances (MeV)
1-4	$p + {}^{12}\mathrm{C}$	g.s.	7.65, 9.64, 10.84, 14.08
5-10	$p + {}^{12}\mathrm{C}$	2^+	11.83, 12.71, 13.35, 14.08, 16.11, 16.57
11-12	$\alpha + {}^9\mathrm{B}$	g.s.	g.s. , 2.36
13	$\alpha + {}^9\mathrm{B}$	2^+	2.79
14-15	$^5\mathrm{Li} + {}^8\mathrm{Be}$	both	g.s.

Table 4.1: A list of the 15 channels that are presently included in the simulation

Most states are described as simple Breit-Wigners, but in the case of $^5\mathrm{Li}$(g.s.), $^8\mathrm{Be}(2^+)$, and $^9\mathrm{B}(2.79)$ penetrability effects are taken into account because these are wide states sitting relatively close to the particle threshold. Angular distributions are generally assumed to be isotropic. Each channel has to be weighted by an appropriate factor to reproduce the relative intensities observed in the experiment. In principle it is straighforward to determine these factors, but many states overlap and consequently a simultaneous normalisation of all channels must be carried out. Basically it boils down to solving a system of 15 linear equations in 15 unknowns. With the simulation properly normalized to the experimental data we can make a direct comparison of the two. Both 3 and 4-particle coincidences are included in the plots.

Figure 4.9 There seems to be a lack of background in the simulation in the upper and the lower end of the cigar-shaped region (which defines the available phase space, when the reaction proceeds through the ^{8}Be ground state). The high intensity diagonal band corresponds to $E_\alpha + E_p = \text{constant}$, i. e. the $^5\mathrm{Li} + {}^8\mathrm{Be}$(g.s.) channel which is easily confirmed with the simulation. Alphas from the $\alpha + {}^9\mathrm{B}(11.65)$

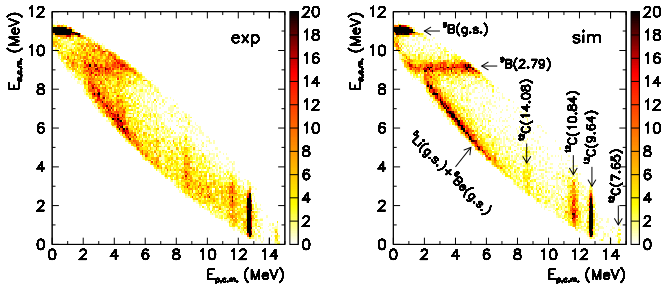

Figure 4.9: Distribution of alpha and proton energies in decays that proceed through the narrow ground state of ^{8}Be. The figure to the left displays the data while the figure to the right shows the results of the simulation.

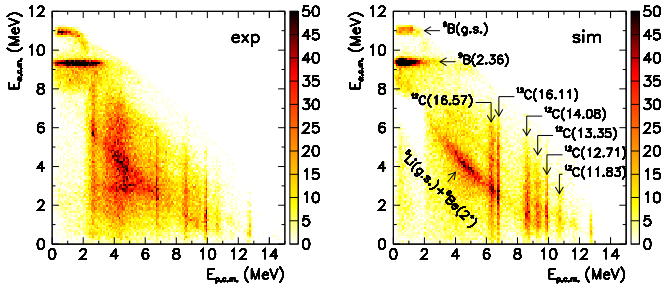

Figure 4.10: Distribution of alpha and proton energies in decays that do *not* proceed through the ground state of ^{8}Be.

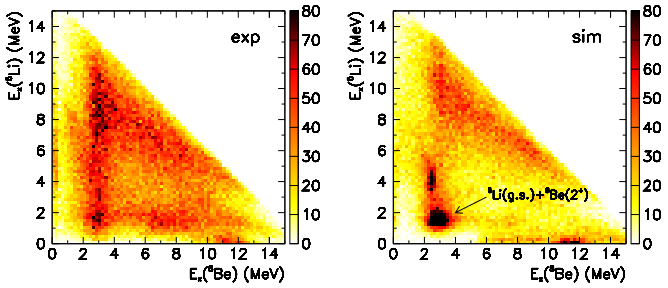

Figure 4.11: Distribution of ^{5}Li and ^{8}Be excitation energies in decays that do *not* proceed through the ground state of ^{8}Be.

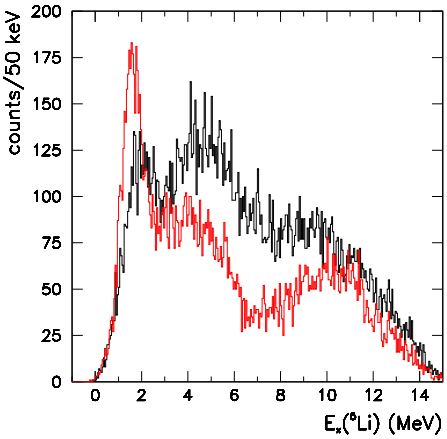

Figure 4.12: ^{5}Li excitation spectrum for decays proceeding through the ground state of ^{8}Be. The data is shown in black and the simulation in red.

channel will have 2.9 MeV in the c. m. frame. The 11.65 MeV state is supposed to be fairly wide, about 800 keV according to [TUNL]. The background excess in the lower end of the cigar could be evidence for this channel.

Figure 4.10 The horizontal band visible in the data at roughly 3 MeV could be due to the 11.65 MeV state in ^{9}B, but could also be caused by accidental coincidences with elastically scattered beam particles (the beam energy is reduced to 2.9 MeV in the c. m. frame). However, in that case one would expect a much more narrow band. Hopefully a study of the timing signals will reveal if these are false or true coincidences. With the amount of statistics collected in this years experiment it will be possible to make a comparison based only on 4-coicidence events in which case false coincidences will not be present. The rectangular area at low proton energies with barely any statistics is reproduced very well in the simulation and is the effect of only triggering on signals in the back detectors. The contribution from the 16.57 MeV and the 13.35 MeV states in ^{12}C have clearly been overestimated in the simulation. Two vertical bands, one wide and one narrow, are visible at low proton energies in the real data, but not in the simulation. These could very well be states in ^{12}C. The high intensity diagonal band is caused by the ^{5}Li(g.s.)+^{8}Be(2^{+}) channel as also verified by the simulation.

Figure 4.11 The intensity of the ^{5}Li(g.s.) + ^{8}Be(2^{+}) spot is too high in the simulation compared to the intensity in the rest of the plot. A high intensity segment is visible just above the ^{5}Li(g.s.) + ^{8}Be(2^{+}) spot in the simulation, but not in the data. These events come from the $\alpha + {}^{9}$B(2.361) channel, which means that the weight given to this channel probably has been overestimated.

Figure 4.12 The position of the ^{5}Li(g.s.) peak is somewhat off, but this could be due to the different background slope on top of which the peak is sitting. The simulation seems to reproduce the trends of the spectrum rather well, most notably the dip around 7 MeV.

All in all the agreement is good. However, there are certainly regions in these plots where the simulation does not reproduce all the statistics actually present in the data. This would seem to suggest that additional channels going through broad intermediate resonances may contribute. We anticipate that the new high-statistics data will allow these resonances to be identified and characterized.

4.8 What can be learned about three-body decays?

Having discussed the general aspects of the ^{10}B(^{3}He, $p\alpha\alpha\alpha$) reaction I will now turn my attention to the $p + {}^{12}$C channel and show how 3 and 4-coincidence events can be used to study the decay mechanism of any intermediate resonance populated in the reaction. My discussion will be limited to the 12.71 MeV state in ^{12}C for two reasons. First it is strongly populated in the ^{10}B(^{3}He, $p\alpha\alpha\alpha$) reaction and offers a good signal-to-background ratio due to its narrow width. Second its decay mechanism has already been studied in great detail in beta-decay experiments so I can check the results of my analysis. Unfortunately the little statistics collected in 2006 renders a similar study of any other state in ^{12}C except from the 9.64 MeV state impossible.

Figure 4.13 has the ^{12}C excitation energy along the first axis while the three alpha energies in the rest frame of the decaying ^{12}C nucleus are plotted on the second axis, i. e. each event is represented by three dots on a vertical line. In decays proceeding through the ^{8}Be ground state the first alpha receives 2/3 of the available energy giving rise to the narrow diagonal band seen in figure 4.13. The two alphas from the break-up of ^{8}Be(g.s.) each emerge with 46 keV, which in the absence of any angular correlations is smeared out into a flat distribution by the motion of the ^{8}Be nucleus.

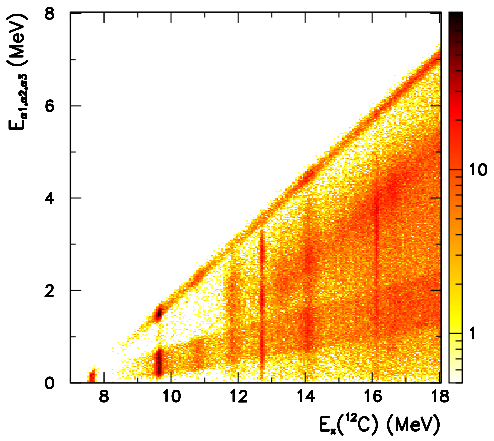

Figure 4.13: Plot including all 3 and 4-coincidence events from the 2.45 MeV data set.

Figure 4.14 shows the alpha energy distribution obtained by gating on the 12.71 MeV state and projecting the three alpha energies on the second axis. The 12.71 MeV state is prevented from decaying through the ^{8}Be ground state due to its unnatural spin-parity, 1^+. Two regions immediately below and above the 12.71 MeV state were used to estimate the background contribution which was then subtracted. In doing so the alpha energies were scaled by a common factor to correct for the small change in available energy when we move up or down in excitation energy. Note that the assumption of a common scaling factor is perfectly legitimate when we consider the background contribution from tails of neighbouring ^{12}C states, while its application to any contribution from the $\alpha + {}^9$B or the ^{5}Li + ^{8}Be channel cannot be justified.

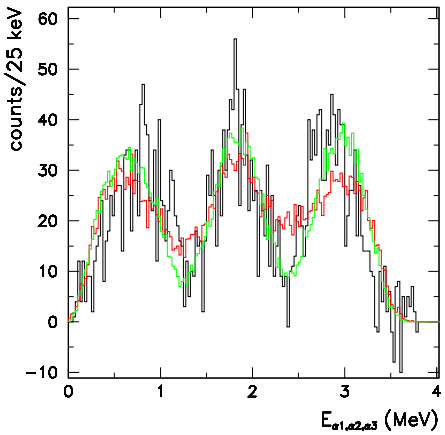

Figure 4.14: Energy distribution of alphas from the decay of the 12.71 MeV state with background subtracted. The data is shown in black, the prediction of the sequential model in red, and the α-cluster model in green.

Two simulations have been superimposed on the data. One assumes a sequential decay through the broad 2^+ resonance in ^{8}Be and includes the $\sin^2(2\theta)$ angular correlation due to angular momentum conservation. The other shows the result of a theoretical calculation based on a 3α-cluster model of ^{12}C in which the Faddeev equations are solved using the adiabatic hyperspherical expansion method [Al07]. Both simulations have been scaled by about 0.10 to yield the same statistics as the data, which explains the reduction in statistical fluctuations. Both simulations reproduce the three-peak profile, but the 3α-cluster model is clearly more succesfull at reproducing the depth of the minima.

However, by including bose symmetry effects in the sequential model its agreement with the data is significantly improved as was shown in [Fy03].

The full kinematics data is nicely presented in a Dalitz plot with the coordinates $\eta_1 = E_1$ and $\eta_2 = (E_1 + 2E_2)/\sqrt{3}$ as shown in figure 4.15, E_1 and E_2 being two randomly chosen final state energies to remove any bias from the data acquisition system. The one-dimensional alpha energy distribution corresponds to the projection of the Dalitz plot onto the second axis. The Dalitz plot does not hold any more information than a regular two-dimensional energy plot of E_1 vs. E_2, but has the advantage that it is symmetric with respect to all three particles. As discussed in [Fy03] effects of Bose symmetry and interactions can be separated to a large extent by studying the radial and angular distribution of points in the Dalitz plot separately.

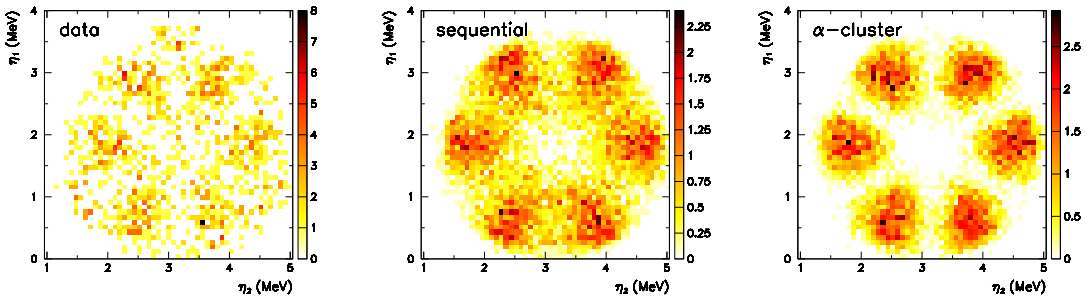

Figure 4.15: Dalitz plots for the decay of the 12.71 MeV state. From left to right: Data, sequential model, and α-cluster model.

The patterns displayed in the Dalitz plot depend on the angular momenta governing the decay, the location and shape of any intermediate resonances, the decay barriers, and the available phase space. However, in the case of a two-step decay certain general features of the Dalitz plot only depend on the ratio of the Q-values as is nicely illustrated in [Fr07]. We anticipate that the high level of statistics obtained in this year's experiment will make it possible to perform similar studies of the decay mechanism of all other known low-lying resonances in ^{12}C.

4.9 A few words on the ^{3}He + ^{7}Li reaction

My analysis of the ^{7}LiF data revealed the existence of various reactions channels due to collisions with ^{7}Li, ^{19}F, ^{12}C from the carbon backing, and a small contamination of ^{6}Li present in the target. The focus of my study was the decay of the $5/2^-$ resonance in ^{9}Be which is populated in the $^3\mathrm{He} + {}^7\mathrm{Li} \rightarrow p + {}^9\mathrm{Be}$ channel. As discussed in chapter 1 this state has a relatively small width to the ^{8}Be ground state, while most of the decays to $n + 2\alpha$ proceed by some other ill-determined mechanism. Unfortunately very little statistics was collected in the 2006 experiment, which made an analysis of the decay-mechanism based on Dalitz plots impossible. However, with the aid of my simulation program I was able to deduce branching ratios to the ^{8}Be ground state which were consistent with litterature values. Comparisons between theoretical cluster calculation and single alpha spectra were also made.

Chapter 5

Outlook (towards ^{8}B)

The preliminary analysis of the new data from this year's experiment has made it clear that we have about two orders of magnitude more 4-coincidence events compared to the 2006 run both for the ^{10}B and the ^{7}Li target. The amount of statistics on the ^{11}B target is of comparable magnitude. Since an extensive toolkit has already been developed in the analysis of the 2006 experiment I anticipate that we will be able to extract many interesting physics results from the new data within short time, this includes studying the decay-mechanism of most ^{12}C states listed in table 1.1, searching for a 2^+ state in the energy region predicted by Morinaga, studying isosping mixing between the 12.71 and 15.11 MeV states, as well as looking for the isobaric analog in ^{9}B to the $1/2^+$ state at 1.68 MeV in ^{9}Be.

While our reaction studies of ^{12}C at CMAM are now coming to an end a new project is already underway. In January this year we performed a measurement of the beta-decay of ^{8}B at the IGISOL facility in Jyväskylä, Finland, with the intention of extracting the neutrino energy spectrum. Knowledge of this spectrum is important for interpreting the results obtained in the solar neutrino experiments Super-Kamiokande, SNO, and ICARUS, which are primarely sensitive to the ^{8}B neutrinos. The beta-decay of ^{8}B may be pictured as a two-step process where ^{8}B beta-decays to ^{8}Be, which subsequently breaks up into two alphas. The shape of the broad alpha-unstable ^{8}Be state formed in the decay must be measured in order to reconstruct the neutrino energy spectrum. At IGISOL the ^{8}B beam was implanted in a very thin carbon foil and the alphas from the subsequent beta-decay were detected in four 16×16 double sided silicon strip detectors. The thickness of the dead layer in the strip detectors is only 100 nm and allowed us to measure alphas with energies as low as 100 keV. The detection of low-energy alphas is important for a correct reconstruction of the high-energy end of the neutrino spectrum. During three days of data taking we observed about 12 million coincidence events. We paid special care to the energy calibration of the detectors, which was done both with standard alpha sources (^{241}Am and ^{215}Po among others) and online with beams of ^{23}Al and ^{20}Na. Two recent measurements of the ^{8}B beta-decay using different techniques give fully consistent results [Wi06, Bh06], but disagree with the results reported in a paper from 2000 [Or00]. With our new measurement we will be able to settle this disagreement. Present evidence points to an error in the 2000 paper.

A major part of the remaining two years of my PhD project will be devoted to the analysis of the data from our experiment in Jyväskylä.

Bibliography

[Al07] R. Alvarez-Rodriguez et al., *Phys. Rev. Lett.* **99** (2007) 072503.

[Ba74] D. P. Balamuth et al., *Phys. Rev. C* **10** (1974) 975-986.

[Ba62] F. C. Barker and P. B. Treacy, *Nucl. Phys.* **38** (1962) 33-49.

[Be03] J. Bency et al., *Phys. Rev. C* **68** (2003) 014305.

[Bh06] M. Bhattacharya et al., *Phys. Rev. C* **73** (2006) 55802.

[Bi53] L. C. Biedenharn and M. E. Rose, *Rev. Mod. Phys.* **25** (1953) 729-777.

[Co58] C. Cook et al., *Phys. Rev.* **111** (1958) 567-571.

[Fi96] R. B. Firestone & V. S. Shirley, *Table of Isotopes*, 8^{th} ed., John Wiley & Sons, 1996.

[Fo06] H. T. Fortune et al., *Phys. Rev. C* **73** (2006) 064302.

[Fr07] M. Freer et al., *Phys. Rev. C* **76** (2007) 034320.

[Fy03] H. O. U. Fynbo et al., *Phys. Rev. Lett.* **91** (2003) 082502.

[Fy05] H. O. U. Fynbo et al., *Nature* **433** (2005) 136-139.

[Ho53] F. Hoyle et al., *Phys. Rev.* **92** (1953) 1095.

[It04] M. Itoh et al., *Nucl. Phys. A* **738** (2004) 268-272.

[Ka07] Y. Kanada-En'yo, *Prog. Theo. Phys.* **117** (2007) 655-680.

[La58] A. M. Lane and R. G. Thomas, *Rev. Mod. Phys.* **30** (1958) 257-353.

[Le86] W. N. Lennard et al., *Nucl. Instrum. Methods A* **248** (1986) 454-460.

[Mo56] H. Morinaga, *Phys. Rev.* **101** (1956) 254-258.

[Mo66] H. Morinaga, *Phys. Lett.* **21** (1966) 78-79.

[Or00] C. E. Ortiz et al., *Phys. Rev. Lett.* **85** (2000) 2909.

[Pa07] P. Papka et al., *Phys. Rev. C* **75** (2007) 045803.

[Pr05] Y. Prezado et al., *Phys. Lett. B* **618** (2005) 43-50.

[Sc66] D. Schwalm and B. Povh, *Nucl. Phys.* **89** (1966) 401-411.

[Te04] O. Tengblad et al., *Nucl. Instrum. Methods A* **525** (2004) 458-464.

[TUNL] TUNL Nuclear Data Evaluation Group, `http://www.tunl.duke.edu/~datacomp/`.

[Wa66] M. A. Waggoner et al., *Nucl. Phys.* **88** (1966) 81-127.

[Wh37] J. A. Wheeler, *Phys. Rev.* **52** (1937) 1083-1106.

[Wi06] W. T. Winter et al., *Phys. Rev. C* **73** (2006) 25503.

[Ya04] T. Yamada, *Phys. Rev. C* **69** (2004) 024309.

[Zi03] J. F. Ziegler et al., *The stopping and range of ions in solids*, Pergamon Press, New York, 2003, program package available at `http://www.srim.org/`.